

RSC Advances



This is an *Accepted Manuscript*, which has been through the Royal Society of Chemistry peer review process and has been accepted for publication.

Accepted Manuscripts are published online shortly after acceptance, before technical editing, formatting and proof reading. Using this free service, authors can make their results available to the community, in citable form, before we publish the edited article. This *Accepted Manuscript* will be replaced by the edited, formatted and paginated article as soon as this is available.

You can find more information about *Accepted Manuscripts* in the [Information for Authors](#).

Please note that technical editing may introduce minor changes to the text and/or graphics, which may alter content. The journal's standard [Terms & Conditions](#) and the [Ethical guidelines](#) still apply. In no event shall the Royal Society of Chemistry be held responsible for any errors or omissions in this *Accepted Manuscript* or any consequences arising from the use of any information it contains.



J name

PAPER

Direct synthesis of graphene from adsorbed organic solvent molecules over copper

Received 00th January 20xx,
Accepted 00th January 20xx

DOI: 10.1039/x0xx00000x

www.rsc.org/

Jinbo Pang,^{ab} Alicja Bachmatiuk,^{ab} Lei Fu,^c Rafael G. Mendes,^b Marcin Libera,^a Daniela Placha,^d Grazyna Simha Martynková,^d Barbara Trzebicka,^a Thomas Gemming,^b Juergen Eckert,^{bfe} and Mark H. Rummeli*^{hg}

The isolation of graphene by Novoselov et al in 2004¹ ignited massive interest in this material. For graphene to succeed fully as a future material its controlled fabrication is required. While numerous routes have been and are being developed, chemical vapor deposition (CVD) is by far the most common approach. There is also interest in forming graphene directly from adsorbed molecules on a substrate. Few examples exist and those that do require multiple steps and rarely offer large graphene domains. In this work we demonstrate a remarkable simple route in which organic solvent precursor molecules are heated in a hydrogen rich atmosphere to directly form graphene over clean Cu foils. The single-step synthesis route has been studied systematically. The systematic studies not only highlight the importance of hydrogen radicals for this reaction, but also provide improved understanding of the role of hydrogen in the formation of graphene from hydrocarbon precursors (e.g. graphene fabrication from thermal CVD).

Introduction

The case for graphene as a future material is strong given its numerous exciting electronic, chemical, mechanical and thermal properties amongst others.^{1–5} To this end there is significant interest in developing fabrication routes as this is key to allow us to truly harness graphene's properties. Numerous routes have been developed. Chemical vapor deposition (CVD) in which hydrocarbons are decomposed over a substrate is perhaps the most popular route since it is a technique commonly adopted by the semiconductor industry and it is also relatively facile to set up in research laboratories. Moreover, the technique is highly successful, particularly when growing graphene over Cu.^{6–8} Another fabrication avenue which also involves metals, but which have a high carbon solubility, is based on carbon dissolving through⁹ or out of the

metal so that the resultant precipitating carbon on the surface forms graphene.^{10–13} Graphene can also be obtained through exfoliation, either through mechanical exfoliation¹ or chemical exfoliation^{14,15} which generally yields graphene oxide which can then be reduced to provide reduced graphene oxide^{16–20}. The synthesis of graphene has also been explored using thermal polymerization such as the polymerization of quinone molecules although this is a somewhat complicated route in that it requires a three step thermal treatment.^{2,3} In another chemo-thermal approach graphene nanoribbons (GNRs) can also be formed through various heating steps from precursor monomers such as 10,100-dibromo-9,90-bianthryl monomers to first dehalogenate the monomers followed by Cyclodehydrogenation.²¹ Aside from CVD and chemo-thermal based routes, solution-based bottom-up approaches have also been shown. They include techniques in which small aromatic hydrocarbons are brought together to form a larger structure (graphene) through coupling reactions.²² A drawback of this technique is that the reduced solubility of large polycyclic systems makes the formation of large graphene domains challenging.²³

In this work, we demonstrate a single-step path to form micron-sized mono-layer and bi-layer graphene flakes over Cu through a remarkably simple chemo-thermal route in which solvent molecules adsorbed on the Cu substrate surface serve as the precursor.

Experimental

Cu substrate pre-treatment

^a Centre of Polymer and Carbon Materials, Polish Academy of Sciences, M. Curie-Skłodowskiej 34, Zabrze 41-819, Poland,

^b IFW Dresden, PO Box 270116, D-01171 Dresden, Germany,

^c College of Chemistry and Molecular Science, Wuhan University, 430072 Wuhan, China,

^d Nanotechnology Centre, VSB-Technical University of Ostrava, 17. listopadu 15, Ostrava-Poruba 708 33, Czech Republic

^e Technische Universität Dresden, Institute of Materials Science, 01062 Dresden, Germany,

^f Center for Advancing Electronics Dresden, TU Dresden, 01062 Dresden, Germany

^g IBS Center for Integrated Nanostructure Physics, Institute for Basic Science (IBS), Daejeon 305-701, Republic of Korea. Email: mark@rummeli.com

^h Department of Energy Science, Department of Physics, Sungkyunkwan University, Suwon 440-746, Republic of Korea.

[†] Electronic Supplementary Information (ESI) available: [SEM on Cu and transferred on SiO₂/Si, thermodynamic calculation, SEM line profile, stats for pressure and flow effect]. See DOI: 10.1039/x0xx00000x

High purity copper foil (25 μm) from Alfa Aesar (99.999%) was used as the substrate. Prior to the chemo-thermal graphene growth the Cu foil was first cleaned. This was achieved heating the Cu foil in air at 800 $^{\circ}\text{C}$ for 30 min. (after which the foil looks black). The oxidized foil was then reduced by heating in an H_2 atmosphere for 30 min at 1025 $^{\circ}\text{C}$.

Direct synthesis of graphene

After this the foil is ready for dip coating in a solvent, a process

implemented an FEI Titan 80/300 cubed instrument with a CEOS image corrector. It was operated at 80 kV. Raman Spectroscopy measurements were conducted using a Renishaw In-Via spectrometer with an excitation laser wavelength of 514 nm.

Calculation of gas equilibrium

Thermodynamic calculations were performed using the NASA computer program CEA (Chemical Equilibrium with

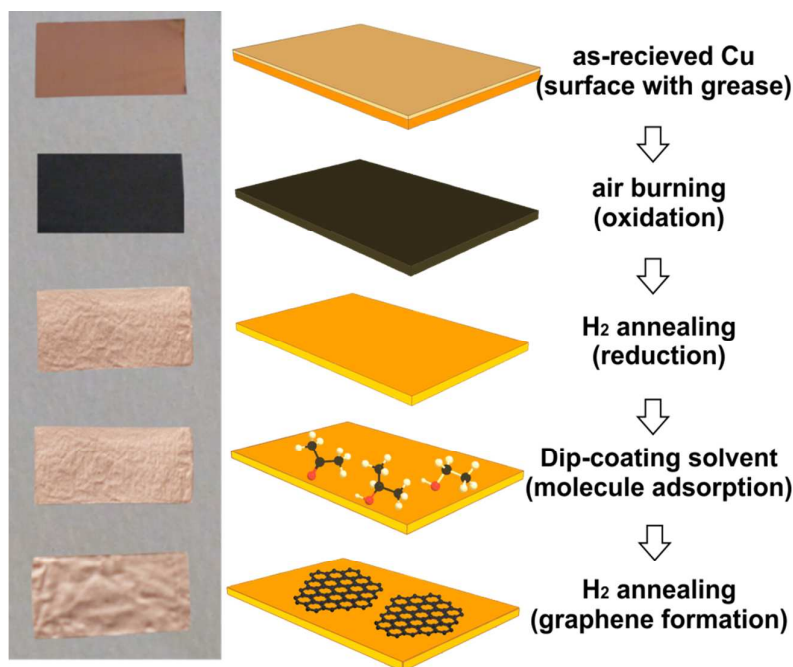


Fig. 1 Illustration showing the foil cleaning steps.

which leaves solvent molecules adsorbed on the surface of the foil. Three solvent, acetone, isopropanol and ethanol were explored. These solvents (VMR international) all have purity of 99.8% for analysis. After dip coating the foil was allowed to dry at ambient conditions. Once dry the foil was loaded into a purpose built horizontal (quartz) tube furnace. The reactions were run in pure H_2 using flow rates between 1 sccm and 100 sccm, pressures from 2 mbar to 1000 mbar and temperatures ranging from 700 $^{\circ}\text{C}$ to 1050 $^{\circ}\text{C}$. The reaction time was 30 min. After the reaction the system cooled to room temperature while in a pure Ar environment (flow 200 sccm). Once cooled the foil was carefully removed and subjected to multiple characterizations.

Characterization

Scanning electron microscope investigations were conducted on a Zeiss Ultra Plus (5kV) and an FEI Quanta FEG 250 (5 kV). Atomic force microscopy measurements were accomplished using a Cypher AFM unit from Asylum Research using the tapping mode with a 1024 by 1024 resolution and a line scan rate of 1.4 Hz. Transmission electron microscopy investigations

Applications). To start with, the constant pressure and constant temperature mode is selected. Then, the initial condition is set with H_2 of ca. 3 μmol and acetone of ca. 0.003 μmol . Next, the same amount isopropanol and ethanol were introduced individually with H_2 in the solvent variant set. The amount of solvent molecules was set to 0.003 mol (modeling the density of adsorbed molecules by, one molecule adsorbing on one Cu atom in a 1 cm^2 Cu surface). Hence, the mole concentration (calculated) for each radical at equilibrium is derived from both reactants.

The equilibrium state is selected at condition of pressure (10 mbar) and temperature (1025 $^{\circ}\text{C}$). For each temperature depending experiments, the corresponding calculation were carried out (700 $^{\circ}\text{C}$ -1050 $^{\circ}\text{C}$). Thus, each calculation was also carried out with variant pressure (2 mbar -1000 mbar). With increasing pressure, the H_2 amount increase from 0.6 μmol to 320 μmol based on $PV=nRT$ equation.

Results and discussion

One-step graphene synthesis from adsorbed molecules

In our facile chemo-thermal route high purity Cu foil is simply dipped in a solvent (or a few solvent drops are dropped on the Cu foil). This leads to organic solvent molecules adhering to the Cu substrate surface. However, prior to deposition of precursor molecules a critical step is to ensure the cleanliness of the Cu foils surface. This is because often the as-received foil has residual grease on the surface that itself can serve as a carbon precursor.²⁴ Various cleaning strategies have been shown including annealing in air²⁵. In our work the most efficient was to burn the foil in air followed by annealing in an H₂ environment (16 sccm). After this no graphene or carbon species were found after thermal treatment in pure Ar or pure H₂ confirming the foil is free from carbon based contaminants. To grow single crystal graphene flakes ca. 1 μm in diameter the

was observed without H₂ being included in the chemo-thermal treatment.

After growth scanning electron microscopy (SEM) and atomic force microscopy (AFM) revealed the formation of numerous graphene flakes on the Cu surface (see Fig. S1 in the supplementary information). For the most part the flakes have six facets, however, at times flakes with 4 facets were observed or they appeared somewhat round. The average size of these flakes varies between 100 nm and just over 1 μm depending on the temperature of the process (discussed later). Closer examination of the flakes by both SEM and AFM show they have wrinkles which is typical of graphene grown over Cu (see Fig. 2).

In addition, in SEM one sees changes in contrast which can be indicative of layer number. Indeed a detailed study (see e.g.

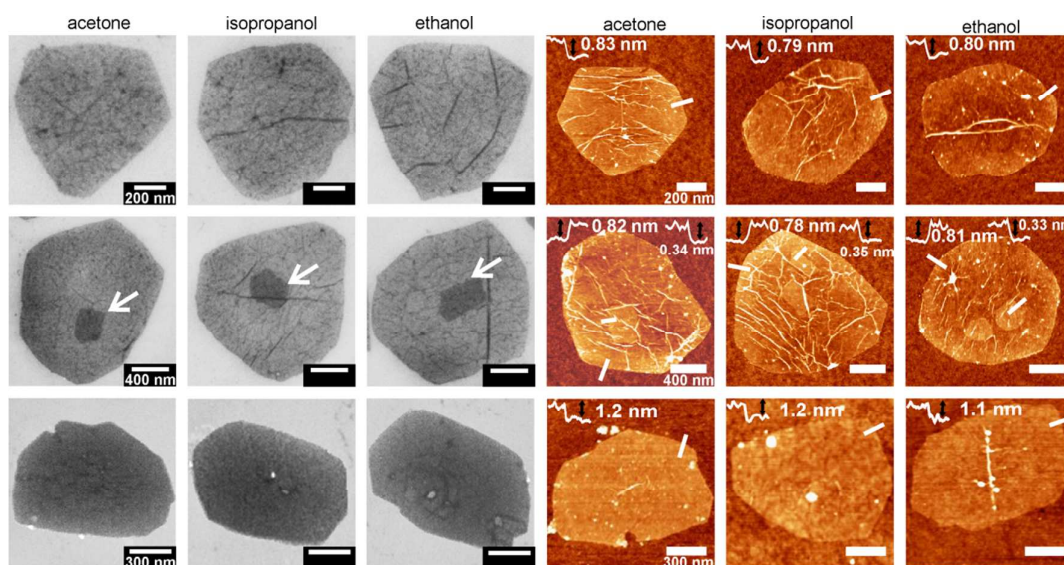


Fig. 2 (from top row to bottom) SEM (left) and AFM (right) micrographs of mono-layer, monolayer with second layer as an island and bi-layer graphene flakes as determined from relative contrast (SEM) or height measurements (AFM).

clean foil was dipped in a solvent (acetone, isopropanol or ethanol) and then left to dry at ambient conditions. EDX measurements of the C loading relative to measured Cu signal (with no measurable C loading) shows C/Cu ratios of 0.3, 0.4 and 0.5 (error 0.1) for acetone, isopropanol and ethanol respectively. In short the carbon loading is similar (within the error). Once dry the foil with precursor molecules was placed in a furnace at temperatures between 700°C and 1025°C with H₂ at a total flow of 16 sccm. The full process is shown schematically in Fig. 1. Graphene growth was only observed between 800°C and 1025°C. A variety of pressures and flow rates were also investigated alongside the temperature studies. No graphene

Fig. S2) suggests the flakes are either monolayer, bi-layer or monolayer with secondary islands on them. The SEM contrast C was determined from:

$$C = (I - I_0) / I_0$$

where I is the measured intensity of the flake and I₀ is the background (substrate) intensity.²⁶ I and I₀ were determined using Gwyddion data analysis software.

The AFM studies in which the heights are measured show homogeneous flakes with heights typically ranging from 0.76 to 0.82 nm and from 1.1 to 1.3 nm concomitant with mono- and Bi-layer graphene. In addition, flakes with islands on them are also observed (right panel Fig. 2).

To confirm these flakes actually are comprised graphene, Raman spectroscopy was implemented. The sp^2 carbon and graphene can relatively easily be determined through Raman spectroscopy through their primary signature modes at ~ 1350 cm^{-1} (D mode), ~ 1600 cm^{-1} (G mode) and ~ 2700 cm^{-1} (2D

In addition to Raman spectroscopy, low-voltage transmission electron microscopy (LVTEM) is an excellent tool with which to characterize graphene.³¹ We conducted numerous LVTEM studies on our samples. Selected area diffraction (SAED) and

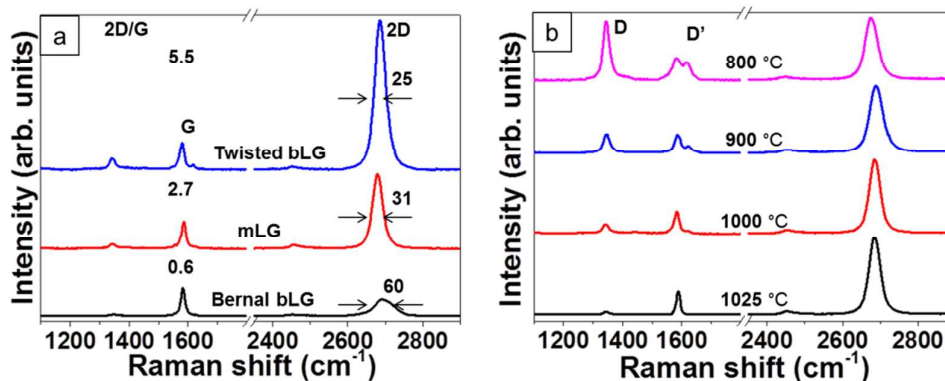


Fig. 3 a. Typical Raman spectra (after transfer to Si/SiO₂ wafers) from flakes for Bernal (A-B) stacked graphene, mono-layer graphene and twisted bi-layer graphene (ca. 20° - 30° rotation). b. Evolution of Raman spectra from graphene with respect to annealing/synthesis temperature. The quality of the graphene improves with increasing temperature.

mode). For all flakes examined (> 150) all three modes are visible as shown in Fig. 3a. In some cases the relative intensity of the G mode and 2D mode (2D/G) lies between 2 and 3 and the 2D mode is relatively narrow and symmetrical. These spectra are attributed to monolayer graphene (e.g. Fig. 3a red spectrum).^{2,27} In other cases the ratio of the 2D/G mode lies between 0.5 and 0.7 while the 2D mode is now asymmetrical and is slightly up-shifted (3 to 5 cm^{-1}) suggesting AB stacked bi-

Fast Fourier Transform data show the three-fold diffraction symmetry of graphene and the reflex spacings for the {10-10} and {11-20} orientations are in agreement with graphene. High resolution TEM micrographs reveal the typical honeycomb lattice of graphene (Fig. 4 a and c) and at times Moiré patterns (Fig. 4b) indicating rotational stacking of graphene were observed.²⁹ Careful counting from the layers with respect to vacuum confirmed the presence of only mono or bi-layer in

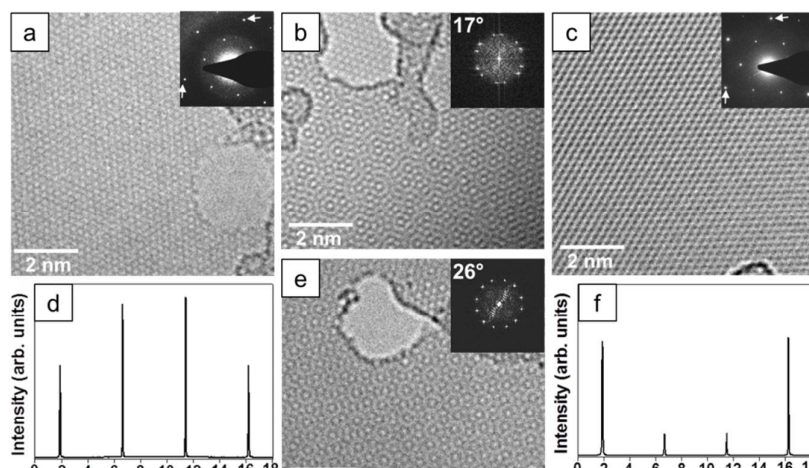


Fig. 4 High resolution TEM micrographs of monolayer graphene (a), twisted bi-layer graphene showing Moiré patterns (b,e) and Bernal (AB) stacked bi-layer graphene (c). Insets: Diffraction information from SAED (a,c) or FFT (b,e). Panels d and f show the relative intensities of the (10-10) and (11-20) reflexes corresponding to monolayer and Bernal bi-layer graphene respectively.

layer graphene (Fig. 3a black spectrum)²⁸ while yet in other cases the 2D/G ratios lie between 5 and 6 and the 2D with the 2D peak also slightly up-shifted.²⁹ This final type of spectrum is associated with non-Bernal stacked or twisted bi-layer graphene with rotational angles between ca. 20° and 30°.³⁰

the sample. Moreover, intensity profiles across the (10-10) and (11-20) reflexes further confirmed the presence of mono- and bi-layer graphene as for example shown in panels d and f of Fig. 4.

Temperature influence and activation energy

We now turn to an examination of the graphene flakes growth with respect to temperature, pressure and flow rate. We begin with temperature variations. For this study the pressure was held at 10 mbar and the flow rate set to 16 sccm.

Temperatures between 700°C and 1050°C were explored. Graphene flakes were only observed for temperatures between 800°C and 1025°C (Fig. 5). By eye one can easily see

organic (precursor) solvent as shown in Fig. 6.

Both the change in diameter and density are linear and allow one to extract the activation energies, E_a , from the Arrhenius plot from the Arrhenius equation:

$$k = Ae^{-E_a/RT}$$

where k is the rate constant of a reaction, A is the prefactor, E_a is the activation energy, R is the universal gas constant and T is the temperature (Kelvin).

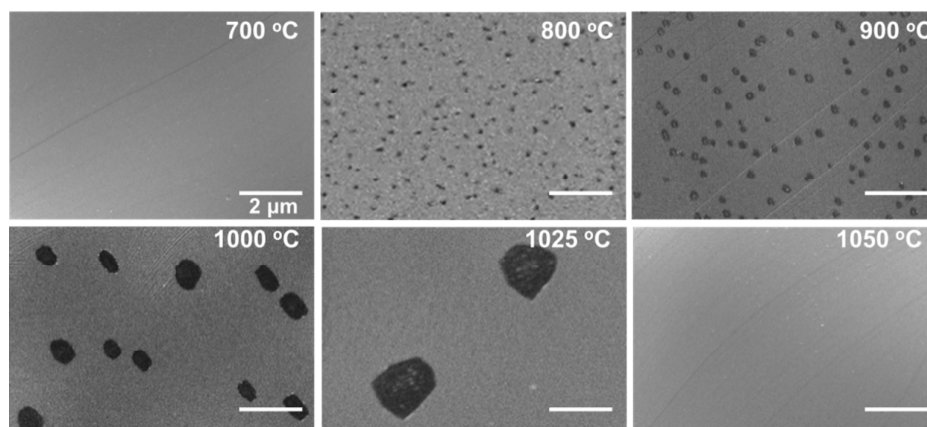


Fig. 5 Representative SEM micrographs showing graphene flake formation and size with reaction temperature. (In these examples acetone molecules were adsorbed on the Cu foil prior to synthesis).

that as the temperature increases from 800°C to 1025°C, the flake sizes increase and the density falls. One can plot both the average flake diameter versus the reciprocal temperature to form an Arrhenius plot for each

The Arrhenius plots in Fig. 6 (top row) shows that the growth rate increases with increasing temperatures (negative slope) and indicates an increase in available carbon species for growth, viz. precursor decomposition and diffusion of

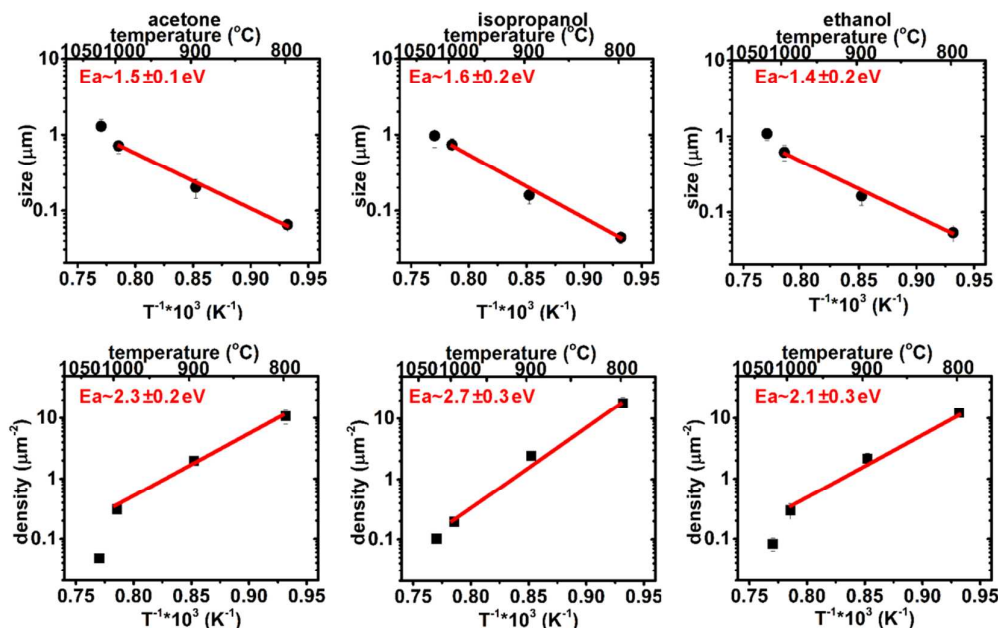


Fig. 6 Arrhenius plots for all three solvents for average diameter (top row) and flake density (bottom row). The activation energies, E_a , are provided in red inside each graph.

molecular/atomic species is increased. The growth activation energies are similar for all three organic solvents explored. It is slightly lower for isopropanol.

The activation energies, E_a , for the change in density with temperature show a positive slope indicating a reduction in graphene island density, and hence a reduction in nucleation site, as temperature increases. This could be attributed to the presence of fewer surface defects on the Cu substrate surface existing with increasing temperature, assuming nucleation occurs at surface defects. In addition, an increase in available C

The effect of reaction pressure was also investigated between 2 mbar and 1 bar with a flow rate of 16 sccm and temperature of 1025 °C. Fig. 7 shows representative SEM data for changes to graphene flake formation with pressure. From 2 mbar to 10 mbar the flake size increases slightly while the density of graphene flakes is at its highest at 5 mbar (Fig. S5 in the supplementary information).

Above pressures of 10 mbar no graphene flakes are observed. Thermodynamic calculations show different changes for H^* , O^* , CH_3 and graphitic C formation with respect to pressure

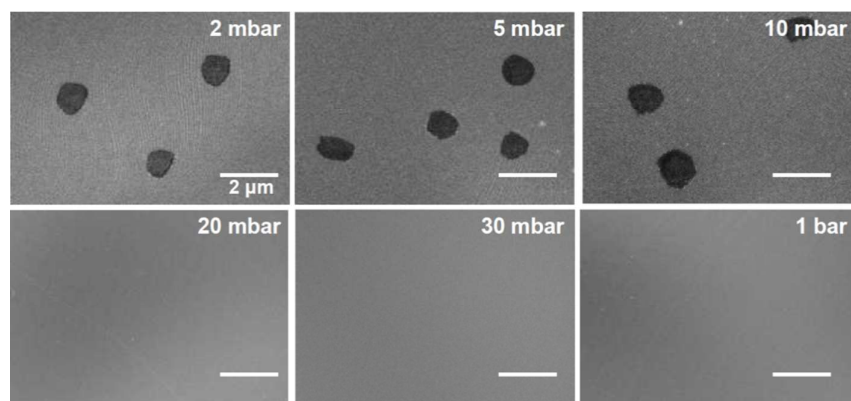


Fig. 7 Representative SEM micrographs of graphene flake formation for different reaction pressures. (In these examples acetone molecules were adsorbed on the Cu foil prior to synthesis).

species for growth, improved species surface diffusion and fewer surface defects with increasing temperature. One might anticipate an increase in surface desorption of species with temperature too. In addition, the number of radicals can also increase with increasing temperatures. Thermodynamic calculations (based on CEA software) show an increase in H^* , O^* , CH_3 and graphitic C (see Fig. S3 in the supplementary information). Indeed studies in which we evaluate the total graphene area with respect to Cu surface area shows an initial increase with temperature to a maximum at around 1000 °C after which it falls (see Fig. S4 in the supplementary information). The initial increase is due to the improved precursor decomposition and surface diffusion, however after 1000 °C etching by radicals and surface desorption of species dominate and the graphene/Cu area ratio decreases.

We also evaluate the changes to the graphene flakes with respect to temperature using Raman spectroscopy (Fig. 3b). At low temperatures the D mode is relatively strong compared to the G mode. Moreover, an additional peak next to the G mode, the so called D' mode, appears at low temperatures and also reduces with increasing temperatures. The D' mode is also related to defects.^{32–34} This indicates that at low temperatures the graphene flakes are rather defective. This might be attributed to the availability of C species for growth not being sufficient to match the growth rate and thus defects such as vacancies will exist.

The role of gas pressure and flow on graphene synthesis

(see figure S7). H^* radicals gradually decrease with pressure and are most prevalent, while CH_3 radicals increase up to ca. 30 mbar and then fall and O^* radicals behave inversely to the CH_3 radicals. Moreover, at ca. 30 mbar graphitic carbon formation is shown to cease. The thermodynamic calculation data changes at higher pressure (ca. 30 mbar) can be described as follows. As the H^* production reduces, the feedstock decomposition aided by H^* is less efficient. At some threshold (around 30 mbar) this change is significant as indicated by the decrease in CH_3 species. In turn this means a significant drop in C species to form sp^2 C. The data shows a change in chemistry such that the number of O^* also increase, which could etch C species further reducing the formation sp^2 C. Although the formation of sp^2 carbon is tied to changes with CH_3 and O^* in the thermodynamic data, their molar fractions are orders of magnitude smaller than for H^* . This suggests H^* radicals are the more important species for sp^2 carbon species formation. This could be attributed to H^* helping decompose the organic solvent precursor molecules (as mentioned above) and also preventing amorphous species formation that can hinder efficient nucleation and growth of graphene flakes.^{2,33,34} In short, the change in pressure leads to changes in chemistry that no longer favour graphitic carbon formation as shown in figure S7 and in agreement with our experimental data.

The role of gas flow was also investigated ($T = 1025$ °C and $P = 2$ mbar). In general, both the average graphene flake size and flake density fall below flow rates of 50 sccm (Fig. S6 in the

supplementary information). Thermodynamics calculations for H*, CH₃ and O* radicals so no real change with respect to flow rate (data not shown).

The formation of bi-layer graphene

Finally we postulate how the bi-layer structures we observe may form. Two key arguments have been show for the growth of bi-layer graphene. In the first gas phase carbon radicals and aromatic fragments are transported just above the surface of the Cu substrate and they may land on a growing graphene flake and enable a second graphene flake to nucleate and grow.³⁵ While in the other scenario carbon radicals and aromatic fragments are able to diffuse between the initial graphene crystal and the underlying substrate and from there nucleate and grow a new flake.³⁷ It is not clear from this data which of these or both are active. Such an investigation is beyond the scope of the current work.

Conclusions

Thus we have shown that mono- and bi-layer graphene flakes up to 1 μm can be grown from organic solvent molecules adsorbed on a clean copper surface. Upon heating the adsorbed feedstock molecules decompose providing active C species for graphene formation. A small flow of H₂ is crucial. The data point to H* radicals playing two key roles. In one it serves as an activator for surface bound C species (i.e. it aids decomposition of the precursor and etches weak carbon bonds at the edges of a growing flake). In the other it can serve as an etchant that can control the graphene flake size and ultimately prevent growth. These roles are similar to those found with conventional thermal CVD of graphene.³⁸ This facile one-step graphene fabrication route may hold promise for the spatial control of graphene fabrication, by, for example, using a mask to control the region where adsorbed feedstock molecules can locate. Moreover, the work provides new insight in to graphene fabrication and the role of hydrogen with respect to hydrocarbon precursors.

Acknowledgements

J.P. thanks the China Scholarship Council (CSC). A.B. thanks the Foundation for Polish Science for the financial support within the frames of the Homing Plus Programme (Grant agreement HOMING PLUS/2013-7/2). The research was supported by the Institute of Basic Sciences (IBS-RO11-D1), Korea and the Sino-German Center for Research Promotion (a). J.E. thanks the German Excellence Initiative via the Cluster of Excellence EXC1056 "Center for Advancing Electronics Dresden" (CfAED).

Notes and references

- 1 K. S. Novoselov, a K. Geim, S. V Morozov, D. Jiang, Y. Zhang, S. V Dubonos, I. V Grigorieva and a Firsov, *Science*, 2004, **306**, 666–9.

- 2 J. H. Warner, F. Schäffel, A. Bachmatiuk and M. H. Rummeli, *Graphene Fundamentals and Emergent Applications*, Elsevier, Waltham, MA, 1st edn., 2013.
- 3 M. H. Rummeli, C. G. Rocha, F. Ortmann, I. Ibrahim, H. Sevincli, F. Börrnert, J. Kunstmann, A. Bachmatiuk, M. Pötschke, M. Shiraishi, M. Meyyappan, B. Büchner, S. Roche and G. Cuniberti, *Adv. Mater.*, 2011, **23**, 4471–4490.
- 4 J. Wu, W. Pisula and K. Müllen, *Chem. Rev.*, 2007, **107**, 718–747.
- 5 J. S. Bunch, A. M. van der Zande, S. S. Verbridge, I. W. Frank, D. M. Tanenbaum, J. M. Parpia, H. G. Craighead and P. L. McEuen, *Science*, 2007, **315**, 490–493.
- 6 X. Li, W. Cai, J. An, S. Kim, J. Nah, D. Yang, R. Piner, A. Velamakanni, I. Jung, E. Tutuc, S. K. Banerjee, L. Colombo and R. S. Ruoff, *Science (80-.)*, 2009, **324**, 1312–1314.
- 7 Y. Hao, M. S. Bharathi, L. Wang, Y. Liu, H. Chen, S. Nie, X. Wang, H. Chou, C. Tan, B. Fallahazad, H. Ramanarayan, C. W. Magnuson, E. Tutuc, B. I. Yakobson, K. F. McCarty, Y.-W. Zhang, P. Kim, J. Hone, L. Colombo and R. S. Ruoff, *Science (80-.)*, 2013, **342**, 720–723.
- 8 L. Fan, Z. Li, X. Li, K. Wang, M. Zhong, J. Wei, D. Wu and H. Zhu, *Nanoscale*, 2011, **3**, 4946.
- 9 G. Ruan, Z. Sun, Z. Peng and J. M. Tour, *ACS Nano*, 2011, **5**, 7601–7607.
- 10 M. H. Rummeli, M. Zeng, S. Melkhanova, S. Gorantla, A. Bachmatiuk, L. Fu, C. Yan, S. Oswald, R. G. Mendes, D. Makarov, O. Schmidt and J. Eckert, *Chem. Mater.*, 2013, **25**, 3880–3887.
- 11 B. Dai, L. Fu, Z. Zou, M. Wang, H. Xu, S. Wang and Z. Liu, *Nat. Commun.*, 2011, **2**, 522.
- 12 X. Liu, L. Fu, N. Liu, T. Gao, Y. Zhang, L. Liao and Z. Liu, *J. Phys. Chem. C*, 2011, **115**, 11976–11982.
- 13 H. Bong, S. B. Jo, B. Kang, S. G. S. K. Lee, H. H. Kim, S. G. S. K. Lee and K. Cho, *Nanoscale*, 2015, **7**, 1314–1324.
- 14 J. H. Warner, M. H. Rummeli, A. Bachmatiuk and B. Büchner, *ACS Nano*, 2010, **4**, 1299–1304.
- 15 X. Li, X. Wang, L. Zhang, S. Lee and H. Dai, *Science*, 2008, **319**, 1229–1232.
- 16 S. Makharza, G. Cirillo, A. Bachmatiuk, I. Ibrahim, N. Ioannides, B. Trzebicka, S. Hampel and M. H. Rummeli, *J. Nanoparticle Res.*, 2013, **15**.
- 17 X. Cui, C. Zhang, R. Hao and Y. Hou, *Nanoscale*, 2011, **3**, 2118–2126.
- 18 K. Coleman and R. S. Edwards, *Nanoscale*, 2013, **5**, 38–51.
- 19 Q. Tang, Z. Zhou and Z. Chen, *Nanoscale*, 2013, **5**, 4541–83.
- 20 S. H. Tamboli, B. S. Kim, G. Choi, H. Lee, D. Lee, U. M. Patil, J. Lim, S. B. Kulkarni, S. Chan Jun and H. H. Cho, *J. Mater. Chem. A*, 2014, **2**, 5077.
- 21 J. Cai, P. Ruffieux, R. Jaafar, M. Bieri, T. Braun, S. Blankenburg, M. Muoth, A. P. Seitsonen, M. Saleh, X. Feng, K. Müllen and R. Fasel, *Nature*, 2010, **466**, 470–473.
- 22 X. Yan and L. Li, *J. Mater. Chem.*, 2011, **21**, 3295.
- 23 D. R. Dreyer, R. S. Ruoff and C. W. Bielawski, *Angew. Chemie - Int. Ed.*, 2010, **49**, 9336–9344.
- 24 S. Gadipelli, I. Calizo, J. Ford, G. Cheng, A. R. Hight Walker and T. Yildirim, *J. Mater. Chem.*, 2011, **21**, 16057.
- 25 C. W. Magnuson, X. Kong, H. Ji, C. Tan, H. Li, R. Piner, C. a. Ventrice and R. S. Ruoff, *J. Mater. Res.*, 2014, **29**, 403–409.
- 26 S. Gupta, E. Heintzman and J. Jasinski, *J. Electron. Mater.*, 2014, **43**, 3458–3469.
- 27 A. C. Ferrari, J. C. Meyer, V. Scardaci, C. Casiraghi, M. Lazzeri, F. Mauri, S. Piscanec, D. Jiang, K. S. Novoselov, S. Roth and A. K. Geim, *Phys. Rev. Lett.*, 2006, **97**, 187401.

Paper

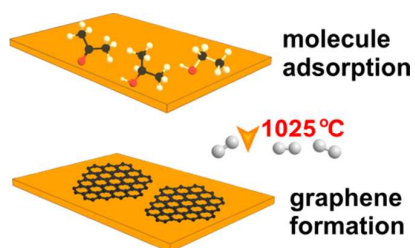
J.name

- 28 L. Liu, H. Zhou, R. Cheng, W. J. Yu, Y. Liu, Y. Chen, J. Shaw, X. Zhong, Y. Huang and X. Duan, *ACS Nano*, 2012, **6**, 8241–8249.
- 29 M. H. Rummeli, S. Gorantla, A. Bachmatiuk, J. Phieler, N. Geißler, I. Ibrahim, J. Pang and J. Eckert, *Chem. Mater.*, 2013, **25**, 4861–4866.
- 30 R. W. Havener, H. Zhuang, L. Brown, R. G. Hennig and J. Park, *Nano Lett.*, 2012, **12**, 3162–3167.
- 31 A. Bachmatiuk, J. Zhao, S. M. Gorantla, I. G. G. Martinez, J. Wiedermann, C. Lee, J. Eckert and M. H. Rummeli, *Small*, 2015, **11**, 515–542.
- 32 F. Banhart, J. Kotakoski and A. V. Krasheninnikov, *ACS Nano*, 2011, **5**, 26–41.
- 33 M. H. Rummeli, A. Bachmatiuk, A. Scott, F. Börrnert, J. H. Warner, V. Hoffman, J.-H. H. Lin, G. Cuniberti and B. Büchner, *ACS Nano*, 2010, **4**, 4206–4210.
- 34 L. G. Cançado, A. Jorio, E. H. M. Ferreira, F. Stavale, C. A. Achete, R. B. Capaz, M. V. O. Moutinho, A. Lombardo, T. S. Kulmala and A. C. Ferrari, *Nano Lett.*, 2011, **11**, 3190–3196.
- 35 I. Vlassioux, M. Regmi, P. Fulvio, S. Dai, P. Datskos, G. Eres and S. Smirnov, *ACS Nano*, 2011, **5**, 6069–6076.
- 36 A. Bachmatiuk, F. Börrnert, V. Hoffmann, D. Lindackers, J.-H. Lin, B. Büchner and M. H. Rummeli, *J. Appl. Phys.*, 2011, **109**, 094317.
- 37 K. Yan, H. Peng, Y. Zhou, H. Li and Z. Liu, *Nano Lett.*, 2011, **11**, 1106–1110.
- 38 Q. Li, H. Chou, J.-H. H. Zhong, J.-Y. Y. Liu, A. Dolocan, J. Zhang, Y. Zhou, R. S. Ruoff, S. Chen and W. Cai, *Nano Lett.*, 2013, **13**, 486–490.

**J name**

PAPER

TOC



20 words: We show the direct synthesis of graphene from adsorbed organic solvent molecules over copper by annealing in hydrogen.

Synopsis: Here we demonstrate the direct synthesis of graphene from adsorbed organic solvent molecules deposited on the surface of copper by simple dip-coating followed by thermal treatment in a hydrogen-rich atmosphere. High quality graphene flakes up to 1 μm can be obtained.